Transmission of visible and near-infrared radiation through a near-field silicon probe

T. I. Kuznetsova* and V. S. Lebedev
P.N. Lebedev Physical Institute, Leninsky prospect 53, Moscow 119991, Russia
(Received 12 February 2004; published 19 July 2004)

We develop a theory of light transmission through the aperture-type near-field optical probe by taking into account the effects associated with light absorption inside its semiconducting core. Our model is based on the exact description of the transverse-magnetic (TM) eigenmodes inside a conical waveguide with perfectly conducting metallic walls. A dissipative matter of its core is described by a complex frequency-dependent dielectric function. Analytical formulas are derived for the energy density distributions of the electric and magnetic fields inside a probe. Particular attention is paid to the evaluation of the near-field transmission coefficient of a metallized silicon probe in the spectral region from 400 nm to 830 nm. We study the dependences of the optical transmittance on the light wavelength, the aperture diameter, the taper angle as well as on the length of the probe. It is shown that the behavior of the electromagnetic fields and the transmission coefficient for the Si probe differ dramatically from the case of a loss-free dielectric core. In this work we point out that the use of a short Si probe instead of a glass one allows us to achieve a strong enhancement in the transmission efficiency in the visible and near-infrared spectral regions.

DOI: 10.1103/PhysRevB.70.035107 PACS number(s): 42.25.Bs, 78.20.Bh, 78.67.−n

I. INTRODUCTION

The intensive development of scanning near-field optical microscopy (SNOM) during the last two decades has already led to enormous progress in studies of different nanoscale phenomena.[1–3] The SNOM technique makes it possible to exceed the classical diffraction limit in optics and to achieve a subwavelength spatial resolution reaching $\sim\lambda/20$. An efficient employment of the aperture-type scanning near-field optical microscope in the "illumination mode" regime is provided by a subwavelength-sized source of radiation (see Ref. 2). Such a source must have a sufficient intensity to achieve an appreciable high signal-to-noise ratio. This quasi-point light source without any background is usually obtained by the use of a metallized fiber probe, tapered to a subwavelength transverse size at its exit, or microfabricated cantilever probe, consisting of solid quartz tip. Although special efforts[4–7] were aimed at increase of the resolution capability of such probes down to $\lesssim 30-40$ nm, their usual spatial resolution is presently about 70–100 nm. This comes as a result of low optical transmission efficiency of the metallized fiber or quartz probes tapered to a small transverse size $d\sim\lambda/20$ (i.e., $\sim$25 nm for a visible light). Therefore, the most serious problem is a simultaneous increase of the transmission efficiency and spatial resolution capability of such optical probes (see Refs. 1 and 2).

As follows from numerical calculations,[8] particularly large values of the transmission efficiency can be achieved when taper angles of near-field probes are large. This conclusion was supported by several experimental works[4,7,12–14] and recent calculations.[9–11] Note that a significant enhancement in the near-field intensity on the probe exit can be achieved by the use of asymmetric structures with a sharp edge at the foot of the probe[15] as well as double-tapered[16,17] and triple-tapered[16] structures. Such structures make it easier to excite the plasmon modes in a metallic coating of the probe. As follows from the available calculations,[8] for an entirely metal-coated probe its resulting optical transmittance can be significantly increased due to the plasmon-supported mechanism of light propagation. It is also worthwhile to recall here several papers devoted to the theoretical consideration of some optical systems involving both a dielectric core and a metallic cladding (see Refs. 18–22). In particular, the authors of Refs. 18 and 22 discussed in details the surface plasmon-polaritons on metal cylinder with dielectric core. Such a cylindrical waveguide is a useful model for the description of optical transmission through a near-field probe with a slightly conical shape.

Another possible way to enhance the optical transmittance through a near-field probe with a subwavelength aperture is the use of a core consisting of a semiconducting matter with a high refractive index n. It is clear that the increase in transmittance with increasing n occurs due to the decrease of light wavelength λ_c inside the core matter. So, for a fixed frequency ω and geometrical parameters of an optical waveguide its critical radius $a_{cr}\propto\lambda_c$ decreases ($\lambda_c=\lambda/n$, where $\lambda=2\pi c/\omega$ is the wavelength in vacuum). Consequently, at high n the cutoff effect, which strongly reduces the light intensity at the exit of an optical probe, affects its transmission efficiency much less than in the case of a glass.

As was pointed out in Refs. 23 and 24, the use of the silicon probes appears very promising for applications of the transmission SNOM technique in the near-infrared (IR) and mid-IR spectral regions, where Si is transparent. This conclusion was supported by a comparative theoretical analysis[25] of the transmission efficiencies of glass and silicon probes in the near-IR region. Numerical calculations were made in Ref. 25 by using the two-dimensional model[19,20] of near-field probes with a small apex angle of 15° at $\lambda=1.3\ \mu$m. Recently, the authors of Ref. 26 have employed a pyramidal silicon probe that was entirely coated with a thin metal film to increase the transmission efficiency in the near-IR region ($\lambda=830$ nm). According to, Ref. 26, the electromagnetic radiation propagating inside the silicon core in the vicinity of the metallic tip is converted into a surface

plasmon mode. An extremely high throughput (up to 2.3%) was achieved in this experiment with the resolution capability of about ≈85 nm.

In the near-IR region the light absorption of Si is small and can be neglected if the probe length is not too large. But in the visible region, the absorption rapidly increases with a decrease of wavelength. Here the losses become important and should be taken into account in order to get an adequate physical pattern of light transmission through a silicon core of a probe. As a result, we have an additional attenuation of the incident optical field, associated with active losses in a dissipative medium. Thus, the gain in the transmission efficiency of a semiconducting core due to its high refractive index may be counterbalanced by the growth of light absorption in the visible spectral region. To deal with these two competing tendencies one needs a detailed theory.

As follows from our recent calculations[27] the use of a near-field probe with the Si core instead of a glass one allows to achieve a strong enhancement in the transmission efficiency not only in the IR but also in the visible spectral range. The major aim of the present work is to elaborate a detailed theoretical model of light transmission through an optical probe by taking into account the effects associated with light absorption inside a core matter and frequency dispersion of its dielectric function. Our consideration is based on the exact analytical description of the conical waveguide eigenmodes inside a probe with a dissipative matter in its core and perfectly conducting metallic walls. A complete theory should additionally include the optical characteristics of a real metallic cladding. However, we concentrate here on a study of a mechanism of light transmission at which the energy is transported only by electromagnetic waves inside a core. A discussion of mechanisms, associated with plasmon-polariton modes in a metallic cladding, is outside the scope of the present work. In the case of a loss-free dielectric core (optical fiber or quartz), a similar analytical approach for the description of light transmission through the conical waveguide, operated in the "illumination mode" regime, has been used in our recent works.[10,11] As in Refs. 10 and 11, our attention here will be focused primarily on calculations of the near-field transmission coefficient associated with the field transformation from the waveguide entrance to the near-field zone at the exit plane.

We consider the transverse magnetic (TM) field modes (i.e., the electric-type waves) throughout this work. The most interesting case corresponds to the TM_{01} mode with the lowest-order indices. For such a mode there are only three field components, which are not equal to zero. This makes it possible to present a theoretical technique for the description of the field transmission through an optical probe in the most compact form and, hence, to concentrate the main attention on a discussion of new effects associated with a dissipative matter in its core. In addition to that for the TM modes there are some specific features of the optical field in the near-field zone at the exit of a probe. For example, at small distances from the cone vertex ($r \ll \lambda$) the energy density associated with the electric field is much greater than that of the magnetic field. Since the electric fields dominate a light-matter interaction this case is of particular important for a SNOM technique. For the dominant transverse-electric field mode (TE_{11}), the study of light transmission through a near-field probe with a silicon core will be the subject of a separate work.

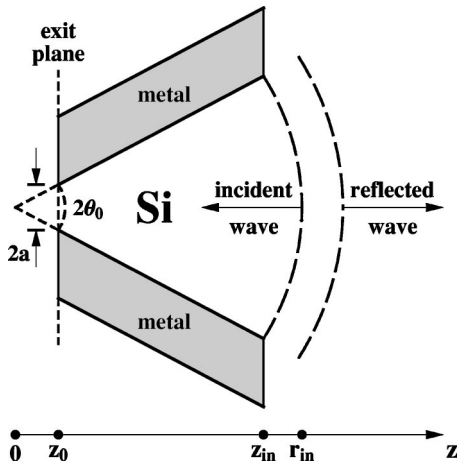

FIG. 1. Schematic illustrating a metal-coated conical waveguide with a silicon core. $2a$ is the aperture diameter, $2\theta_0$ is the cone angle, z_0 is the longitudinal coordinate at the waveguide exit, r_{in} and $z_{in}=r_{in}\cos\theta_0$ are the radial and longitudinal coordinates at the waveguide entrance, respectively.

Our calculations cover a wide range of light wavelengths and geometrical parameters of the silicon probe including the most interesting case of large taper angles and sufficiently small aperture diameter reaching $\sim\lambda/20$. It is natural that a high spatial resolution capability of an optical probe can be achieved only for a small exit aperture. However, a practical limit to spatial resolution of the aperture-type metallized probes is determined by the penetration depth of the electromagnetic field into the metallic cladding (see Ref. 2).

The paper is organized as follows. First, we describe our theoretical approach and present basic formulas for the electromagnetic fields and energy density distributions inside a cone, including some asymptotic expressions at small and large distances from its vertex as compared to the wavelength in a core medium (Secs. II and III). In Sec. IV we consider the behavior of the near-field transmission coefficient as a function of the geometrical parameters of a probe and the characteristic length of light absorption inside its core. Section V contains the results and discussions of our calculations for the TM_{01} eigenmode inside the metallized cone with a silicon core. In Sect. VI we present the conclusions.

II. FORMULATION OF THE PROBLEM. TRANSVERSE-MAGNETIC WAVES

We consider here time-harmonic electromagnetic fields inside a cone whose core consists of a dissipative medium and whose walls are perfectly conducting (see Fig. 1). As noted previously, here we are interested in the field, which is transverse magnetic with respect to the radial coordinate r. To construct this field in spherical coordinates (r,θ,φ) we must take the magnetic vector potential $\mathbf{A}$ with only one nonzero component $A_r \equiv U(r,\theta,\varphi)$ (i.e., $A_\theta = A_\varphi = 0$), and

choose the electric vector potential to be equal to zero.[28] Here r is the distance from the cone vertex, and θ and φ are the polar and azimuthal angles, respectively. According to Ref. 28 the basic equation for the U-function has the form

$$\frac{\partial^2 U}{\partial r^2} + \frac{1}{r^2}\left[\frac{1}{\sin\theta}\frac{\partial}{\partial\theta}\left(\sin\theta\frac{\partial U}{\partial\theta}\right) + \frac{1}{\sin^2\theta}\frac{\partial^2 U}{\partial\varphi^2}\right] + k^2 U = 0. \tag{1}$$

For a dissipative matter, the wave number k in Eq. (1) is complex:

$$k = \frac{\omega}{c}\sqrt{\varepsilon\mu}, \quad \sqrt{\varepsilon\mu} = n + i\kappa. \tag{2}$$

Here $\omega = 2\pi c/\lambda$ is the frequency, c is the velocity of light, and λ denotes its wavelength in vacuum, and n and κ are the refractive index and the attenuation coefficient, respectively. Assuming the permeability $\mu = 1$, the real and imaginary parts of the frequency-dependent dielectric function $\varepsilon(\omega) = \varepsilon'(\omega) + i\varepsilon''(\omega)$ can be written as

$$\varepsilon' = n^2 - \kappa^2, \quad \varepsilon'' = 2n\kappa. \tag{3}$$

For the electric-type (transverse magnetic, TM) waves considered in the present paper, the field components can be expressed in terms of the U-function by means of the following relations:[28]

$$E_r = \frac{\partial^2 U}{\partial r^2} + \frac{\omega^2(\varepsilon' + i\varepsilon'')}{c^2}U, \quad E_\theta = \frac{1}{r}\frac{\partial^2 U}{\partial r\,\partial\theta},$$

$$E_\varphi = \frac{1}{r\sin\theta}\frac{\partial^2 U}{\partial r\,\partial\varphi}, \tag{4}$$

$$H_r = 0, \quad H_\theta = -\frac{i\omega(\varepsilon' + i\varepsilon'')}{c}\frac{1}{r\sin\theta}\frac{\partial U}{\partial\varphi},$$

$$H_\varphi = \frac{i\omega(\varepsilon' + i\varepsilon'')}{c}\frac{1}{r}\frac{\partial U}{\partial\theta}. \tag{5}$$

Note that E_r, E_θ, E_φ and H_r, H_θ, H_φ mean the projections of electric **E** and magnetic **H** fields onto the corresponding axes of spherical coordinates (r, θ, φ). For the electric-type waves, the boundary condition at an interface between a core and perfectly conducting metallic coating of a waveguide can be written as

$$U(r, \theta, \varphi)\big|_{\theta=\theta_0} = 0, \tag{6}$$

where θ_0 is the cone half-angle (see Fig. 1). This condition yields $E_r(\theta_0) = 0$, and $E_\varphi(\theta_0) = 0$ for the tangential components of the electric field **E** at $\theta = \theta_0$.

The relevant (nonsingular at $r \to 0$) solution of Eq. (1) has the form

$$U(r, \theta, \varphi) = \mathcal{R}(r) P_\nu^m(\cos\theta) e^{im\varphi}, \tag{7}$$

$$\mathcal{R}(r) = C r j_\nu\left[(n + i\kappa)\frac{\omega r}{c}\right], \tag{8}$$

at which the radial dependence $\mathcal{R}(r)$ of the vector potential (7) is expressed through the spherical Bessel function of the first kind $j_\nu(z)$ with the index ν not equal to an integer. Here C is a constant. Expression (8) describes the standing wave with vanishing amplitude at the cone vertex ($r = 0$). The dependence on the polar angle θ is determined by the associated Legendre function (see Ref. 29) of the first kind $P_\nu^m(\cos\theta)$ with power ν and order m (m is an integer).

At large distances from the cone vertex ($r \gg 1/|k|$), the asymptotic expression for the radial part of the vector potential (8) can be written as

$$\mathcal{R} \approx \frac{C}{2i(\omega/c)(n + i\kappa)}\left\{\exp\left[-\kappa\frac{\omega r}{c} + i\left(n\frac{\omega r}{c} - \frac{\pi\nu}{2}\right)\right] - \exp\left[\kappa\frac{\omega r}{c} - i\left(n\frac{\omega r}{c} - \frac{\pi\nu}{2}\right)\right]\right\}. \tag{9}$$

This expression describes two waves traveling in the opposite directions, with the amplitudes differing by the factor $\exp(-2\kappa\omega r/c)$. For the nondissipative medium ($\kappa = 0$) the asymptotic expression (9) at $r \gg c/n\omega$ is reduced to an especially simple form:

$$\mathcal{R}(r) \approx \frac{C}{(n\omega/c)}\sin\left(n\frac{\omega r}{c} - \frac{\pi\nu}{2}\right). \tag{10}$$

The radial dependence of the $\mathcal{R}$ function in the vicinity of the cone vertex ($r \ll (c/\omega)/|n + i\kappa|$) is determined by the power law

$$\mathcal{R}(r) \approx \frac{C\sqrt{\pi}}{2^{\nu+1}\Gamma(\nu + 3/2)}\left[\frac{\omega(n + i\kappa)}{c}\right]^\nu r^{\nu+1}. \tag{11}$$

It is evident from Eq. (11) that the field amplitude rapidly drops with a decrease of the radial coordinate and vanishes at $r = 0$.

With the help of Eq. (7), the boundary condition (6) can be rewritten in terms of the associated Legendre function (see Ref. 28)

$$P_\nu^m(\cos\theta_0) = 0. \tag{12}$$

Each choice of numbers m ($m = 0, 1, 2, \ldots$) and s ($s = 1, 2, 3, \ldots$) in this equation determines a possible TM_{ms} field mode [s denotes the number of the corresponding root of Eq. (12) such that $\nu_{m1} < \nu_{m2} < \nu_{m3} < \cdots$]. The eigenvalues ν_{ms} of Eq. (12) depend upon the cone half-angle θ_0, such that ν_{ms} increases as the θ_0 value decreases. For the lowest-order mode ($s = 1$, $m = 0$) numerical solutions of Eq. (12) are given in Ref. 11 for several magnitudes of the cone half-angle $\theta_0 = \pi/24$, $\pi/12$, $\pi/6$, $\pi/4$, $\pi/3$, and $\pi/2$.

In the present paper we shall consider only the lowest-order electric-type wave, i.e., the TM_{01} mode with $m = 0$ and $s = 1$. In this case $\partial U/\partial\varphi = 0$ and we have only three field components, E_r, E_θ, and H_φ, which are not equal to zero [see (4), (5), and (7). Substituting Eq. (7) into (4) and (5) we get

$$E_r = \frac{\nu(\nu+1)}{r^2}\mathcal{R}(r)P_\nu(\cos\,\theta), \tag{13}$$

$$E_\theta = \frac{1}{r}\frac{\partial\mathcal{R}(r)}{\partial r}\frac{\partial P_\nu(\cos\,\theta)}{\partial\theta}, \tag{14}$$

$$H_\varphi = i\frac{\omega(\varepsilon'+i\varepsilon'')}{c}\frac{1}{r}\mathcal{R}(r)\frac{\partial P_\nu(\cos\,\theta)}{\partial\theta}, \tag{15}$$

where $P_\nu(\cos\,\theta)$ is the Legendre function of the first kind and order ν (see Ref. 29).

III. ENERGY DENSITY DISTRIBUTIONS INSIDE A METALLIZED CONE WITH A LOSSY MATTER IN ITS CORE

In dissipative media with frequency-dependent dielectric function $\varepsilon=\varepsilon'+i\varepsilon''$ and permeability $\mu=\mu'+i\mu''$, the general expressions (see Ref. 30) for the time-averaged densities of the electromagnetic energy $w_{el}=w_r+w_\theta$, and $w_m=w_\varphi$ are given by

$$w_{el} = \frac{1}{16\pi}\frac{d(\omega\varepsilon')}{d\omega}(|E_r|^2+|E_\theta|^2), \tag{16}$$

$$w_m = \frac{1}{16\pi}\frac{d(\omega\mu')}{d\omega}|H_\varphi|^2, \tag{17}$$

where $\varepsilon'=\Re e\{\varepsilon\}$ and $\mu'=\Re e\{\mu\}$. The total time-averaged energy density of the electromagnetic field is $w_{tot}=w_{el}+w_m$. To determine the near-field transmission coefficient of a truncated conical waveguide (see below Sec. V) we also introduce the following quantities:

$$W_\beta(r) = 2\pi r^2\int_0^{\theta_0} w_\beta(r,\theta)\sin\,\theta\,d\theta, \tag{18}$$

which represent the integrals of w_r, w_θ, or w_φ taken over a part of spherical surface lying inside the cone ($0\leqslant\theta\leqslant\theta_0, 0\leqslant\varphi\leqslant 2\pi$) at a given distance r from the cone vertex. Equation (18) can be rewritten as

$$W_\beta(r) = 2\pi r^2(1-\cos\theta_0)\langle w_\beta(r)\rangle, \tag{19}$$

where $\langle w_\beta\rangle$ denotes the energy density of the corresponding field component ($\beta=r,\theta,\varphi$), averaged over the polar angle.

With the help of relations (7) and (8), (13)–(18), the integral energy density W_β can be evaluated explicitly. The resulting expression for the integral energy density W_r is given by

$$W_r(r) = \frac{|C|^2}{8}\frac{d(\omega\varepsilon')}{d\omega}[\nu(\nu+1)]^2\mathcal{I}_\nu^{(1)}\left|j_\nu\left[(n+i\kappa)\frac{\omega r}{c}\right]\right|^2, \tag{20}$$

where $\mathcal{I}_\nu^{(1)}$ is the angular integral,

$$\mathcal{I}_\nu^{(1)} = \int_0^{\theta_0}[P_\nu(\cos\,\theta)]^2\sin\,\theta\,d\theta. \tag{21}$$

The expression for the W_θ component can be obtained if we use the recurrence relation for the derivative of the spherical Bessel function. Then, using Eqs. (8), (14), (16), and (18), we get

$$W_\theta(r) = \frac{|C|^2}{8}\frac{d(\omega\varepsilon')}{d\omega}\mathcal{I}_\nu^{(2)}\left|(\nu+1)j_\nu\left[(n+i\kappa)\frac{\omega r}{c}\right] - \left[(n+i\kappa)\frac{\omega r}{c}\right]j_{\nu+1}\left[(n+i\kappa)\frac{\omega r}{c}\right]\right|^2. \tag{22}$$

The angular integral $I_\nu^{(2)}$ in (22) can be directly expressed in terms of (21),

$$\mathcal{I}_\nu^{(2)} = \int_0^{\theta_0}\left[\frac{\partial P_\nu(\cos\,\theta)}{\partial\theta}\right]^2\sin\,\theta\,d\theta = \nu(\nu+1)\mathcal{I}_\nu^{(1)}. \tag{23}$$

Similarly, by using Eqs. (8), (15), (17), and (18) we obtain the expression for the azimuthal component of the integral energy density,

$$W_\varphi(r) = \frac{|C|^2|\varepsilon'+i\varepsilon''|^2}{8}\left(\frac{\omega r}{c}\right)^2\mathcal{I}_\nu^{(2)}\left|j_\nu\left[(n+i\kappa)\frac{\omega r}{c}\right]\right|^2. \tag{24}$$

The total density of electromagnetic energy inside a cone, integrated over $2\pi r^2\sin\,\theta\,d\theta$ ($0\leqslant\theta\leqslant\theta_0$, $0\leqslant\varphi\leqslant 2\pi$), can now be evaluated as

$$W_{tot}(r) = 2\pi r^2\int_0^{\theta_0} w_{tot}(r,\theta)\sin\,\theta\,d\theta = W_r(r)+W_\theta(r)+W_\varphi(r). \tag{25}$$

At small distances from the cone vertex compared to the light wavelength $\lambda_c=\lambda/n$ in the core medium ($r\ll\lambda_c$), the basic expressions (20), (22), and (24) for the integral energy densities of various field components can be expanded in power series of $|k|r$. Then, the resulting expression for the integral energy density $W_{tot}(r)$, summarized over all field components (25) takes the form

$$W_{tot}(r) \approx \xi_\nu\frac{|C|^2\mathcal{I}_\nu^{(2)}}{16}\frac{d(\omega\varepsilon')}{d\omega}\left(|n+i\kappa|\frac{\omega r}{c}\right)^{2\nu}. \tag{26}$$

Here ξ_ν is a constant,

$$\xi_\nu = \frac{\pi(\nu+1)(2\nu+1)}{2^{2\nu+1}\Gamma^2(\nu+3/2)}, \tag{27}$$

whose magnitude is determined by the eigenvalue $\nu\equiv\nu_{01}(\theta_0)$ of the TM_{01} mode. Note that the main contribution to Eq. (26) is determined by the energy density of the electric field. This fact directly follows from the simple relation $\langle w_m\rangle/\langle w_{el}\rangle\propto(|k|r)^2$ for the ratio of the energy density of the magnetic field to that of the electric field at $r\ll 1/|k|$.

Expressions for the integral energy densities W_r, W_θ, and W_φ at distances from the cone vertex much greater than the wavelength in the core medium ($r \gg \lambda_c$), directly follow from the corresponding general formulas (20)–(24) with a help of the asymptotic expression for the spherical Bessel function $j_\nu(z)$ with a complex argument. Here we present the final asymptotic expressions only for the integral energy densities of electric, $W_{el}=W_r+W_\theta$, and magnetic, $W_m \equiv W_\varphi$, fields:

$$W_{el} \approx \frac{|C|^2}{16}\frac{d(\omega\varepsilon')}{d\omega}\mathcal{I}_\nu^{(2)} \times \left[\cosh\left(2\kappa\frac{\omega r}{c}\right) + \cos\left(2n\frac{\omega r}{c} - \pi\nu\right)\right], \tag{28}$$

$$W_m \approx \frac{|C|^2}{16}|\varepsilon' + i\varepsilon''|\mathcal{I}_\nu^{(2)} \times \left[\cosh\left(2\kappa\frac{\omega r}{c}\right) - \cos\left(2n\frac{\omega r}{c} - \pi\nu\right)\right]. \tag{29}$$

The asymptotic expression for the integral density of the total electromagnetic energy $W_{tot}=W_{el}+W_m$ inside the cone with a dissipative medium in its core has the form

$$W_{tot} \approx \frac{|C|^2}{16}\mathcal{I}_\nu^{(2)}\left\{\left[\frac{d(\omega\varepsilon')}{d\omega} + |\varepsilon|\right]\cosh\left(2\kappa\frac{\omega r}{c}\right) + \left[\frac{d(\omega\varepsilon')}{d\omega} - |\varepsilon|\right]\cos\left(2n\frac{\omega r}{c} - \pi\nu\right)\right\}. \tag{30}$$

As follows from (30), the integral energy density $W_{tot}(r)$ as a function of the radial coordinate r exhibits an oscillatory behavior at distances far from the cone vertex $r \gg c/\omega|n+i\kappa|$. These oscillations are the result of the frequency-dependent dielectric function; they are absent if the core is made of a loss-free medium ($\varepsilon'=$const and $\varepsilon''=0$). Then, in accordance with Refs. 10 and 11, the asymptotic expressions (28)–(30) take a particularly simple form at large distances from the cone vertex $r \gg c/n\omega$:

$$W_{el} \approx \frac{|C|^2\varepsilon}{8}\mathcal{I}_\nu^{(2)}\cos^2\left(\frac{n\omega r}{c} - \frac{\pi\nu}{2}\right), \tag{31}$$

$$W_m \approx \frac{|C|^2\varepsilon}{8}\mathcal{I}_\nu^{(2)}\sin^2\left(\frac{n\omega r}{c} - \frac{\pi\nu}{2}\right), \tag{32}$$

$$W_{tot} \approx \frac{|C|^2\varepsilon}{8}\mathcal{I}_\nu^{(2)}. \tag{33}$$

For a lossy matter the amplitudes of the electric [$W_{el} \propto d(\omega\varepsilon')/d\omega$, Eq. (28) and magnetic [$W_m \propto |\varepsilon|$, Eq. (29) components of the integral energy densities are unequal and can significantly differ from each other. We illustrate this fact in Fig. 2 by presenting the wavelength dependences of the real part, ε', of the dielectric function of silicon and the corresponding effective value of $\varepsilon'_{eff}=d(\omega\varepsilon')/d\omega$ in spectral region from 400 nm to 830 nm. Therefore, the oscillations of the electric and magnetic components of the integral energy density do not compensate each other far from the cone vertex, and this results in the appearance of nonvanishing oscillations in the radial dependence of the total sum of $W_{tot}=W_{el}+W_m$. According to Eqs. (28) and (29) the ratio of the oscillating and monotonic components of the integral energy density W_{tot} is determined by the factor

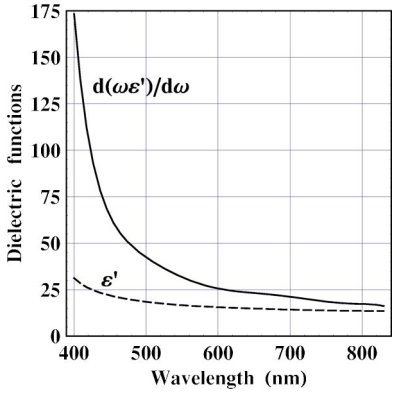

FIG. 2. The real part ε' of the dielectric function (dashed curve) of Si obtained by interpolating experimental data Ref. 35 and the effective value $\varepsilon'_{eff}=d(\omega\varepsilon')/d\omega$ (full curve) versus the wavelength in vacuum λ.

$$\gamma(\omega) = \frac{d(\omega\varepsilon')/d\omega - |\varepsilon|}{d(\omega\varepsilon')/d\omega + |\varepsilon|} \approx \frac{\omega d\varepsilon'/d\omega}{2\varepsilon' + \omega d\varepsilon'/d\omega}. \tag{34}$$

The second approximate equality in Eq. (34) is valid if the losses, associated with light absorption, are not too large such that $\varepsilon'' \ll \varepsilon'$.

As follows from (34), the value of γ turns out to be small ($\gamma \ll 1$), when the dispersion of the dielectric function is sufficiently small ($\omega d\varepsilon'/d\omega \ll \varepsilon'$). Then, the amplitude of the oscillating component of the integral energy density $W_{tot}(r)$ at large distances from the cone vertex ($r \gg \lambda_c$) is small, so that this effect can be neglected [see Eqs. (31)–(33)]. This is the case of a near-field probe with a glass or a quartz core. In the opposite case of large dispersion $\omega d\varepsilon'/d\omega \gg \varepsilon$, the value of (34) becomes approximately equal to $\gamma \approx 1$. So, the amplitude of the oscillating component of the integral energy density $W_{tot}(r)$ becomes large. This is the case of a near-field semiconducting probe with a substantial influence of light absorption in the core matter.

The integral energy density $W_{tot}(r)$ far from the cone vertex $r \gg \lambda_c$, averaged over the oscillations in Eq. (30), takes the form

$$\overline{W}_{tot} \approx \frac{|C|^2}{16}\mathcal{I}_\nu^{(2)}\left[\frac{d(\omega\varepsilon')}{d\omega} + |\varepsilon|\right]\cosh(r/r_\kappa). \tag{35}$$

Here r_κ is the attenuation length:

$$r_\kappa = c/2\kappa\omega = \lambda/4\pi\kappa. \tag{36}$$

For a loss-free matter the expression (35) is reduced to (33).

It is important to stress that in the presence of a dissipation there is a significant difference in magnitudes of the energy fluxes associated with the forward and the backward waves:

$$S_f(r) = \frac{c\overline{W}_{tot}(r)}{n}\frac{\exp(r/r_\kappa)}{\exp(r/r_\kappa)+\exp(-r/r_\kappa)}, \tag{37}$$

$$S_b(r) = -\frac{c\overline{W}_{tot}(r)}{n}\frac{\exp(-r/r_\kappa)}{\exp(r/r_\kappa)+\exp(-r/r_\kappa)}. \tag{38}$$

Their ratio $|S_b/S_f|$ is equal to $\exp(-2r/r_\kappa)$. Expressions (35), (37), and (38) are valid provided that a distance from the cone vertex significantly exceeds the radiation wavelength in the core $r \gg \lambda_c = c/n\omega$.

IV. THE NEAR-FIELD TRANSMISSION COEFFICIENT OF A CONICAL WAVEGUIDE

A. Basic expression

Let us now discuss the problem of light transmission through a conical waveguide. It is well known that for propagating time-harmonic waves, the transmission coefficient is defined in terms of the energy flux (more precisely, it is a ratio of the transmitted intensity to the incident intensity of electromagnetic field, see, e.g., Ref. 28). In the case of an optical probe tapered to a subwavelength-sized diameter, we deal with nonpropagating waves. In this situation it is necessary to distinguish a near-field transmission coefficient of a waveguide and the transmission coefficient to the far-field zone (see Ref. 2). The evaluation of the far-field transmission coefficient includes a consideration of the field transformation from the waveguide exit to the far-field zone in free space. A consideration of this stage of the field transformation is somewhat similar to the well-known problem[31,32] of diffraction by a small aperture (see Ref. 33 for the so-called hypergeometric waveguide, and Ref. 34 for the conical geometry).

The near-field transmission coefficient, T, can be expressed in terms of the time-averaged energy densities associated with the output and the input fields of the waveguide. For spherical waves, it can be defined as the ratio,[11]

$$T = \frac{W_{tot}^{out}}{W_{tot}^{in}}, \tag{39}$$

of the time-averaged energy density $W_{tot}^{out} \equiv W_{tot}(z_0)$ at the exit plane $z=z_0$ of a truncated cone (see Fig. 1) integrated over the aperture cross section:

$$W_{tot}^{out} = 2\pi\int_0^a w_{tot}(\rho, z_0)\rho d\rho,\ a = z_0 \tan\theta_0, \tag{40}$$

to the corresponding integral energy density W_{tot}^{in} at the waveguide entrance. The total energy density $w_{tot}=w_r+w_\theta+w_\varphi$ in Eq. (40) can be evaluated with the use of expressions (16) and (17), in which the field components E_r, E_θ, and H_φ should be taken at the exit plane $z=z_0$ of the waveguide.

In dissipative media, the basic expression for the near-field transmission coefficient, T, of an optical probe should be somewhat modified compared to the case of a loss-free medium (see Refs. 10 and 11). It can be defined by the relation (39), in which the integral energy density at the exit aperture (W_{tot}^{out}) is given by Eq. (40), while the value of W_{tot}^{in} has the form

$$W_{tot}^{in} = \alpha 2\pi r_{in}^2\int_0^{\theta_0} w_{tot}(r_{in},\theta)\sin\theta\, d\theta. \tag{41}$$

Here r_{in} is the input value of the radial coordinate, i.e. the distance from the cone vertex to the waveguide entrance (see Fig. 1). The integration performed in Eq. (41) includes the part of the spherical surface ($r=r_{in}$, $0\leqslant\theta\leqslant\theta_0$, $0\leqslant\varphi\leqslant 2\pi$) corresponding to the input value of $r=r_{in}$. The factor α is defined by the relation

$$\alpha(\omega, r_{in}) = \left|\frac{(n/c)S_f(r_{in})}{\overline{W}_{tot}(r_{in})}\right| = \frac{1}{1+\exp[-2r_{in}/r_\kappa(\omega)]}. \tag{42}$$

It shows a fraction of the energy density of the electromagnetic field at the waveguide entrance, associated with the forward wave alone. So, the contribution coming from the backward wave turns out to be completely removed. It can be seen from (42) that the magnitude of α varies from $1/2$ to 1 at all possible values of the parameter r_{in}/r_κ. For a loss-free medium it is equal to $1/2$. However, for a lossy medium we obtain $\alpha\to 1$, provided that the distance r_{in} from the cone vertex becomes considerably greater than the attenuation length r_κ.

B. Simple expressions for a small exit hole

When the aperture diameter $2a$ is significantly less than the light wavelength $\lambda_c=\lambda/n$, one can use the simple expressions (26) for the integral energy density W_{tot} at the exit of a conical waveguide, $r_{out}=a/\sin\theta_0$. For the integral energy density $W_{tot}(r_{in})$ at the waveguide entrance that corresponds to large distances from the vertex ($r_{in}\gg\lambda_c$) we use the asymptotic expression (35) with $r=r_{in}$. Then, using the definition of the near-field transmission coefficient of a waveguide [see Eqs. (39)–(41), we obtain the simple formula

$$\mathcal{T} \approx \chi_\nu\beta\left(\frac{2a|1+i\kappa/n|}{\lambda_c\sin\theta_0}\right)^{2\nu} e^{-r_{in}/r_\kappa}. \tag{43}$$

Here

$$\beta = \frac{2d(\omega\varepsilon')/d\omega}{d(\omega\varepsilon')/d\omega+|\varepsilon|} \tag{44}$$

and

$$\chi_\nu = \frac{\pi^{2\nu+1}(\nu+1)(2\nu+1)}{2^{2\nu}\Gamma^2\left(\nu+\frac{3}{2}\right)} \tag{45}$$

are the dimensionless coefficients; $\lambda_c=\lambda/n$ is the light wavelength in the core matter; and r_{in} is the distance from the cone vertex ($r=0$) to the waveguide entrance, which is practically equal to the length of the probe $l\approx r_{in}$ at small aperture radius a. It is seen that the β coefficient (whose value is of the order of unity) is determined by the frequency disper-

sion of the dielectric function. The χ_ν coefficient strongly depends on the value of $\nu(\theta_0)$ such that its value decreases with an increase of the taper angle θ_0.

Rigorously speaking, the transmission coefficient $\mathcal{T}=W_{tot}(r_{out})/W_{tot}^{in}$, determined by simple expression (43), is slightly differed from (39). This is because the integration in Eq. (26) for $W_{tot}(r_{out})$ is performed over the part of the spherical surface at $r=r_{out}$ [see Eq. (25)], while in Eqs. (39) and (40) the integration is fulfilled over the exit plane $z=z_0$ ($z_0=r_{out}\cos\theta_0$, Fig. 1). However, as was shown in Ref. 10 this leads to a small difference in numerical coefficients but does not change the dependences on the main physical parameters such as the aperture diameter, the refractive index, and the attenuation length.

Note also that for the applications to near-field optical microscopy the most interesting case corresponds to the situation in which the light transmission through a probe with a semiconducting matter in its core occurs far from the peak in its absorption band. Then the real part ε' of the dielectric function of the core is much greater than its imaginary part ε'', and, hence $\kappa \ll n$. In the opposite case, the light absorption inside a core of a probe is too large and the resulting transmittance is very small. Nevertheless, assuming $\kappa \ll n$ it is necessary to distinguish the two limiting cases that correspond to different relationships between the attenuation length r_κ and the length of the probe r_{in}.

When a dissipation of the electromagnetic energy inside a core of a probe is very small ($r_{in} \ll r_\kappa$), the light absorption can be neglected. This situation is typical for the transmission of the optical radiation through a probe with a glass core. Therefore, one can put $\exp(-r_{in}/r_\kappa)\approx 1$ in Eq. (43). Moreover, for a loss-free medium the frequency dispersion of the dielectric function is negligible, i.e., $d(\omega\varepsilon')/d\omega \approx \varepsilon'$. Hence, β is practically equal to unity. Then, the near-field transmission coefficient (43) takes the form

$$\mathcal{T} \approx \chi_\nu \left(\frac{2a}{\lambda_c \sin\theta_0} \right)^{2\nu}. \tag{46}$$

This expression describes the major features of light transmission through the subwavelength-sized exit hole in a loss-free conical waveguide. It is seen from (46) that when we consider the case of small aperture radius ($a \ll \lambda_c$), the near-field transmission coefficient is strongly dependent on the ratio a/λ_c. To clarify its dependence on the taper angle it is important to recall that eigenvalues ν_{01} of the lowest-order TM_{01} mode exhibit rapid fall with an increase of the θ_0 value. For example, $\nu_{01}=8.681$, 4.083, 2.548, 1.777, and 1 at $\theta_0=\pi/12$, $\pi/6$, $\pi/4$, $\pi/3$, and $\pi/2$, respectively (see Refs. 10 and 11). Therefore, the transmission coefficient strongly grows as the taper angle increases.

In the opposite limiting case of large active losses inside a semiconducting core ($l \gg r_\kappa$), the near-field transmission coefficient (43) is proportional to the exponentially small factor $\exp(-l/r_\kappa)$. This reflects the strong influence of light absorption inside a core on the transmittance of an optical probe. Another important point is the strong dependence of the transmission coefficient on the refractive index of the core matter. At $\kappa/n \ll 1$, this dependence is practically the same as in the case of a loss-free dielectric core ($\mathcal{T} \propto n^{2\nu}$). As a result, a considerable increase in the value of n for a semiconducting core compared to a glass one can provide a substantial enhancement in the resulting transmittance, even in the presence of an appreciable absorption of light inside a probe.

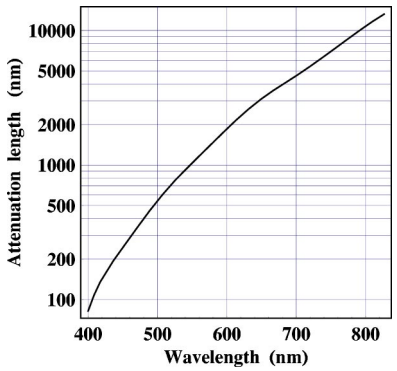

FIG. 3. The attenuation length r_κ (36) for Si as a function of light wavelength in vacuum λ.

V. RESULTS AND DISCUSSIONS

A. Optical fields inside a conical waveguide with a silicon core

Let us discuss the main features of the optical fields inside a conical waveguide with a silicon core (see Fig. 1). According to available experimental data,[35] the refractive index n of Si increases monotonically from 3.67 to 5.57 in spectral region from $\lambda=830$ nm ($\hbar\omega=1.5$ eV) down to $\lambda=400$ nm ($\hbar\omega=3.1$ eV). This is considerably larger than for a glass or quartz ($n\approx 1.55$). At the same time, the attenuation coefficient κ grows from 0.005 to 0.387 in the same spectral region, so that the ratio of κ/n is changed from 1.4×10^{-3} to 6.9×10^{-2}. The wavelength dependence of the attenuation length r_κ is shown in Fig. 3.

In Fig. 4 we illustrate the main features in the radial dependences of the angular-averaged energy densities of the

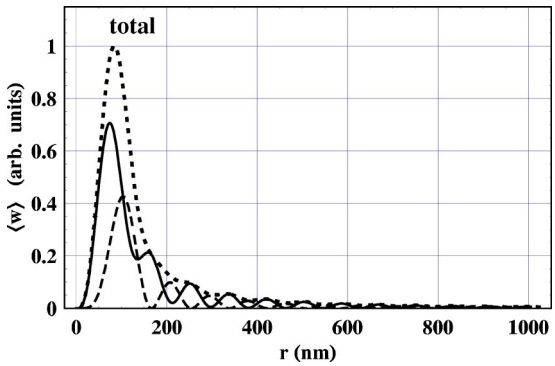

FIG. 4. The normalized energy densities of the electric ($\langle w_{el}\rangle$, full curve) and magnetic ($\langle w_m\rangle$, dashed curve) fields inside a metal-coated cone with a silicon core as functions of the distance from the cone vertex r. The dotted curve is the radial dependence of the total energy density, $\langle w_{tot}\rangle=\langle w_{el}\rangle+\langle w_m\rangle$. Calculations represent the results for the TM_{01} eigenmode at $\lambda=633$ nm; the cone angle $2\theta_0$ is equal to $\pi/2$.

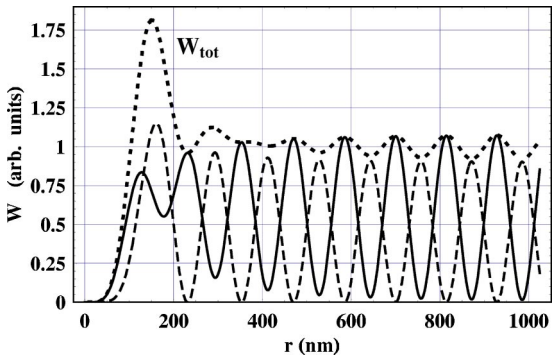

FIG. 5. The distributions of the integral energy densities of the electric (W_{el}, full curve) and magnetic (W_m, dashed curve) fields inside a cone with a silicon core as functions of the radial coordinate r. The dotted curve is the radial dependence of their sum, $W_{tot}=W_{el}+W_m$. Calculations represent the results for the TM_{01} eigenmode at $\lambda=830$ nm; the cone angle $2\theta_0$ is equal to $\pi/2$.

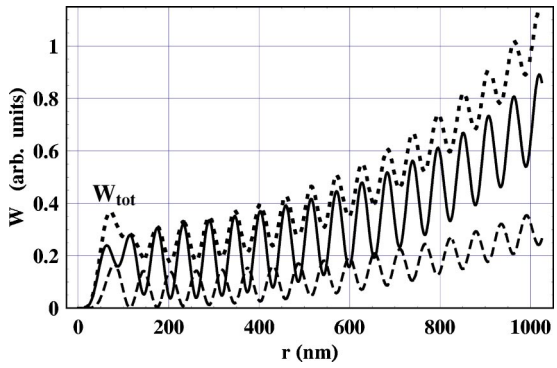

FIG. 6. The same as Fig. 5, but for $\lambda=488$ nm.

electric $\langle w_{el}\rangle$ (full curve) and magnetic $\langle w_m\rangle$ (dashed curve) fields inside a silicon probe for the radiation wavelength $\lambda=633$ nm ($\lambda_{Si}=163$ nm). Calculations have been performed for the lowest-order TM_{01} eigenmode by using the general formulas of Sec. III; the cone angle $2\theta_0$ was taken to be equal to $\pi/2$. It is evident that at large distances from the cone vertex ($r\gg\lambda_{Si}$) oscillations corresponding to the electric and magnetic fields turn out to be opposite in phase. At small $r\ll\lambda_{Si}$, the drop of the magnetic field with a decrease of the radial coordinate occurs much rapidly than that of the electric field. Therefore, the energy density near the cone vertex is mainly determined by the contribution of the electric field, $\langle w_{el}\rangle\gg\langle w_m\rangle$.

The radial dependence of the total energy density $\langle w_{tot}\rangle=\langle w_{el}\rangle+\langle w_m\rangle$ is shown in Fig. 4 by the dotted curve. One can see that it exhibits a clearly pronounced maximum in the range of $r\sim\lambda_{Si}/2$. This points to the strong concentration of the electromagnetic energy inside the conical waveguide. The subsequent rapid drop of the total energy density reflects the evanescent nature of the electromagnetic field in the region of the subwavelength transverse sizes of the waveguide.

A quite different influence of light absorption on the field behavior in the near-IR and the short-wavelength part of the visible spectrum becomes evident from a comparison of our results in Figs. 5 and 6. These figures represent the radial dependences of the integral density of the total electromagnetic energy ($W_{tot}=W_r+W_\theta+W_\varphi$, dotted curves) inside a cone with a silicon core, obtained for the two different values of the radiation wavelength: $\lambda=830$ nm and $\lambda=488$ nm; the cone angle $2\theta_0$ is equal to $\pi/2$. The calculations have been performed for the TM_{01} field-mode using Eqs. (20)–(25). Since the attenuation coefficient of Si in the near-infrared region ($\lambda=830$ nm) is very small, the radial dependence of the integral energy density $W_{tot}(r)$ (Fig. 5) is similar to the previously considered case of a glass core (see Fig. 4 in Ref. 11). The new feature is the presence of nonvanishing oscillations of $W_{tot}(r)$ in the asymptotic region ($r\gg\lambda_{Si}$). In accordance with the discussion in Sec. III, these oscillations result from the frequency dispersion of the dielectric function of Si (in contrast to the optical fiber, where $\varepsilon\approx\text{const}$). At $\lambda=830$ nm the ratio (34) of the oscillating and monotonic components of the integral energy density W_{tot} far from the cone vertex ($r\gg\lambda_{Si}$) is equal to $\gamma=0.093$. Note however, that the behavior averaged over these nonvanishing oscillations is qualitatively similar to that of the glass fiber.

The other situation takes place for the short wavelength part of the visible spectrum due to the significant increase of the attenuation coefficient κ of Si. For example, at $\lambda=488$ nm the value of the attenuation coefficient κ becomes 17.6 times greater than that for $\lambda=830$ nm. This leads to a substantial common reduction of the integral energy density W_{tot} (dotted curve in Fig. 6) as the distance from the cone vertex decreases from large magnitudes of $r\gg\lambda_{Si}$ ($r=1000$ nm in our example) down to $r\sim\lambda_{Si}\approx\lambda/n_{Si}=112$ nm at $\lambda=488$ nm. This behavior is accounted for by the dissipation of the electromagnetic energy inside the silicon core such that $\overline{W}_{tot}\propto\cosh(r/r_\kappa)$ at $r\gg\lambda_{Si}$ [see Eq. (35)]. In addition to that in the short wavelength part of the visible spectrum there is a great increase in amplitude of the oscillating (nonvanishing at $r\gg\lambda_{Si}$) component of $W_{tot}(r)$ as compared to the near-IR range (see Figs. 5 and 6). The ratio (34) of the oscillating and monotonic components of the integral energy density becomes equal to $\gamma=0.41$ at $\lambda=488$ nm.

As in Fig. 5, there is an appreciable peak in the radial dependence of the integral energy density $W_{tot}(r)$ in the range of $r\sim\lambda_{Si}/2$ (see Fig. 6). At small $r\lesssim\lambda_{Si}/2$ the drop of the integral energy density is primarily determined by the power law [see Eq. (11)]. This power drop of the total electromagnetic energy is typical for light transmission through a subwavelength-sized exit hole in a conical waveguide (see Refs. 10 and 11). This is the dominant effect at sufficiently small r in both cases of the loss-free dielectric core and the lossy semiconducting core of near-field probes.

It is important to note that all expressions for the optical fields and numerical calculations presented above (see Figs. 4–6) have been obtained for a closed cone with a metal coating. Since the real probe is a truncated cone, one needs to estimate perturbations of the fields associated with the truncation. In our recent works[10,11] we outlined a technique for the evaluation of this effect and made some numerical estimates. They demonstrate that such perturbations are small if the aperture diameter $2a\ll\lambda/2$. Similar estimates for the silicon probe confirm this conclusion. Therefore, we can apply the expressions, derived in Secs. II and III, for calcu-

lations of the optical transmittance through the subwavelength-sized aperture of a near-field silicon probe.

B. Transmittance of a near-field probe with a silicon core

We present here the results of our calculations of the near-field transmission coefficient of the metallized silicon probe as a function of the wavelength of the incident radiation λ. All calculations have been made for the TM_{01} mode by Eqs. (39)–(41) and the general expressions (20), (22), and (24) for the integral energy density W_{tot} inside a cone with a dissipative matter in its core. They cover all visible and near-IR spectral regions and a set of the aperture diameters $2a$ (25, 50, 70, and 100 nm). The results obtained for the most interesting case of large taper angles $2\theta_0=\pi/3$ and $\pi/2$ are shown in Figs. 7 and 8, respectively. To demonstrate a dependence of light absorption inside the Si core on the probe length, we calculated the transmission coefficient T for various values of $l=2$, 4, and 8 μm [figures a, b, and c, respectively).

As expected, the values of T are strongly dependent on the aperture diameter and the taper angle in full agreement with simple formula (26) derived in this work. The situation here is qualitatively similar to that for an optical fiber probe. In other words, the near-field transmission coefficient exhibits a strong drop as the aperture diameter decreases from 100 nm down to 25 nm (see curves 1, 2, 3, and 4 in Figs. 7 and 8). At the same time, an increase of the full taper angle of a probe leads to an increase in the transmission efficiency.

However, the wavelength dependence of the near-field transmission coefficient, obtained in the present work for the Si probe differs dramatically from the case of a glass fiber (or some other loss-free material in the core). As is evident from Figs. 7 and 8, the transmittance of the Si probe strongly varies over spectrum. If the length of the probe is not too large $l \lesssim 8$ μm, the transmission coefficient first increases with the decrease of the wavelength in the IR region, reaches its maximum at a definite wavelength λ_{max} in the visible or near-IR range, and then strongly falls at $\lambda \ll \lambda_{max}$ in the short-wavelength part of the visible spectrum. The position of the maximum λ_{max} and the maximal value of T_{max} depends on the specific geometrical parameters of the probe.

The key point is that this maximum in the transmission efficiency of a silicon probe lies in spectral region $\lambda \sim 550-800$ nm. It is important to stress that this occurs despite the fact that the value of the attenuation coefficient of Si considerably increases in the visible region compared to the near-IR one. For example, at $\lambda=663$ nm (the wavelength of He/Ne laser), $\lambda=532$ nm (second harmonic of YAG laser), and $\lambda=488$ nm (the wavelength of argon-ion laser), the respective values of the attenuation coefficient κ for Si become equal to 1.90×10^{-2}, 5.06×10^{-2}, and 8.57×10^{-2} instead of $\kappa=4.88\times10^{-3}$ at $\lambda=830$ nm (the wavelength of laser diode used in Ref. 26). The respective magnitudes of the attenuation length (36) turn out to be equal to $r_\kappa=2.66$ μm, 0.84 μm and 0.45 μm at $\lambda=633$ nm, 532 nm, and 488 nm, instead of 13.53 μm at $\lambda=830$ nm.

It is seen from Figs. 7 and 8 that the wavelength dependences of the transmission coefficient are qualitatively similar to each other for different values $2\theta_0=60°$ and $2\theta_0=90°$ of the full taper angle. Therefore, we discuss below carefully our results for $2\theta_0=90°$ because the absolute values of T in this case are larger. At $\lambda=830$ nm the near-field transmission coefficient is equal to $T=2.9\times10^{-4}$, $T=9.2\times10^{-3}$, $T=4.7\times10^{-2}$ and $T=2.4\times10^{-1}$ for the aperture diameter $2a=25$ nm, 50 nm, 70 nm, and 100 nm, respectively. These results correspond to the length of the probe edge $l=2$ μm [Fig. 8(a)]. On the whole, in the near-IR region the effect of light absorption inside the Si probe is sufficiently weak. Nevertheless, at $\lambda=830$ nm an increase of the probe length from

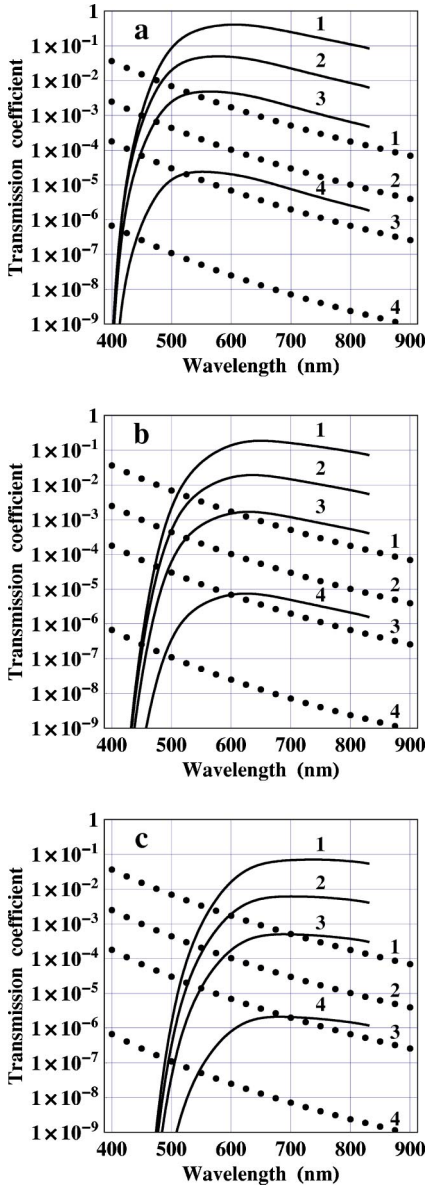

FIG. 7. The near-field transmission coefficients, $T=W_{tot}^{out}/W_{tot}^{in}$, of the conical waveguide with a silicon core (full curves) and a glass core (dotted curves) as a function of the wavelength in vacuum λ. Curves 1, 2, 3, and 4 are the present calculations for the TM_{01} eigenmode at the aperture diameter $2a=100$ nm, 70 nm, 50 nm, and 25 nm, respectively. The cone angle $2\theta_0$ is equal to 60°. Figures (a), (b), and (c) correspond to various lengths of the probe $l=2$, 4, and 8 μm, respectively.

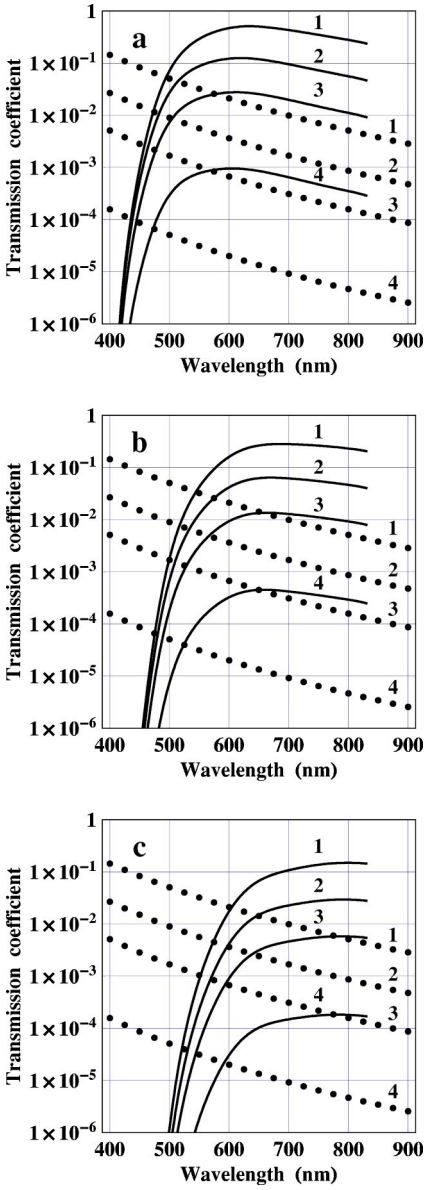

FIG. 8. The same as Fig. 7, but for the cone angle $2\theta_0=90°$.

2 up to 10 μm leads to a decrease of the T values for about 1.8 times. This clearly indicate the necessity of incorporation the imaginary part of the dielectric function of Si in calculations of the optical transmittance of a near-field probe even in the near-IR region.

For the probe length $l \lesssim 4$ μm, the near-field transmission coefficient reaches its maximum at $\lambda \sim 600-650$ nm. For the wavelength $\lambda=633$ nm, our calculations at $l=2$ μm yield: $T=9.2\times10^{-4}$, $T=2.3\times10^{-2}$, $T=1.2\times10^{-1}$ and $T=5.1\times10^{-1}$ for the aperture diameter $d=25$ nm, $d=50$ nm, $d=70$ nm, and $d=100$ nm, respectively. It is important to note that this is about two–three times larger than that at $\lambda=830$, depending on the specific value of the aperture diameter. At $l \lesssim 4$ μm, the rapid drop in the transmission coefficient occurs in spectral region $\lambda \lesssim 500-550$ nm [see Figs. 8(a) and 8(b)] so that the values of T becomes small only in the short wavelength part of the visible spectrum. However, at $l=8$ μm [Fig. 8(c)] the rapid drop of T starts from $\lambda \sim 600$ nm.

Further we illustrate the advantage in the use of a silicon probe in comparison with conventional fiber ones for the transmission SNOM technique. We compare the present estimates of the near-field transmission coefficient for Si with those obtained previously for a glass with small n (see the dotted curves in Figs. 7 and 8). Although the taper angles of fiber probes do not usually exceed 40° (see, e.g., Ref. 2 and references therein), which additionally restricts their efficiency, we use here the value $2\theta_0=90°$ and $n_{glass}=1.55$ to make a comparison with our recent results.[11]

For the probe with the length $l=2$ μm, the aperture diameter $2a=50$ nm, and the taper angle $2\theta_0=90°$ we get $T_{Si}/T_{glass}=2.2$, 14, 45, and 71 for $\lambda=488$ nm, 532 nm, 633 nm, and 830 nm, respectively. For the same length and the aperture diameter, but for the taper angle $2\theta_0=60°$ we have $T_{Si}/T_{glass}=43$, 240, 800, and 960. One can see that in the latter case the enhancement in the optical transmittance turns out to be considerably larger than for $2\theta_0=90°$. This fact is in full agreement with the simple analytic formula (43), according to which $T \propto n^{2\nu(\theta_0)}$ (where $\nu=4.083$ and 2.548 for the TM_{01} mode at $2\theta_0=60°$ and 90°, respectively). However, the case of $2\theta_0=90°$ is more interesting due to especially high absolute magnitudes of T (see Fig. 8).

It is important to stress that an enhancement occurs not only in the near-IR but also in the visible spectral region. Moreover, as we have already discussed above the maximum in the transmission coefficient of a near-field Si probe lies in the range $\lambda=600-650$ nm for $l \lesssim 4$ μm. According to our theory, the enhancement occurs as a result of competition between two factors: the rise of n and the decrease of the attenuation length r_κ [see Eq. (43)]. Our calculations demonstrate that the former factor is more important in most parts of the visible spectrum. However, a strong enhancement in the transmittance of a near-field silicon probe in the visible range is possible provided the probe length is sufficiently short (no more than several micrometers). Then the effects associated with the light absorption inside the Si core are not too strong.

VI. CONCLUSIONS

(1) We have developed a theoretical model for the description of the electromagnetic waves inside an optical probe with a dissipative matter in its core. The core is described by a complex frequency-dependent dielectric function; the walls of the conical waveguide are perfectly conducting. The model was applied for the evaluation of the energy density distributions inside an optical probe with a semiconducting (Si) core. The formulas derived in this work contain our previous analytical results for a near-field optical probe with a loss-free dielectric core[10,11] as a special case.

(2) According to our theory the fields behavior inside the Si probe differs essentially from the case of the conventional fiber probe. A new feature in the radial dependence of the integral energy density is the field attenuation, associated with light absorption. This leads to a significant difference in the energy fluxes of the forward and backward waves inside

a probe. It was shown that the total energy density of electromagnetic field inside a cone with the Si core exhibits oscillations, which do not vanish even at large distances from the cone vertex.

(3) The emphasis of this work has fallen on the evaluation of the near-field transmission coefficient of the Si probe in all visible and near-IR spectral regions. For a subwavelength-sized exit hole, we have derived a simple expression (43) for the transmission coefficient of a conical waveguide with a lossy dielectric core. It provides the explicit dependences of T on the wavelength λ, the aperture diameter $2a$, the taper angle θ_0 as well as on the length of the probe l, the refractive index n, and the attenuation length r_κ. It was shown that for the Si probe the wavelength dependence of the transmission coefficient differs dramatically from the case of a loss-free dielectric core [for which T increases monotonically as $(a/\lambda)^{2\nu}$ with a decrease of λ. On the contrary, the transmission coefficient for Si exhibits a nonmonotonic dependence on the wavelength. It grows with a decrease of λ in the IR region, then reaches its maximum, and rapidly drops in the short-wavelength part of the visible spectrum. The key point is that this maximum lies at $\lambda \sim 550-800$ nm for a short Si probe, $l \lesssim 5$ μm (see Figs. 7 and 8).

(4) As follows from our calculations, at large taper angles ($2\theta_0 \sim 60°-90°$) high values of the transmission coefficient can be achieved for passage of the optical radiation through the Si core of a probe. We have made a comparison of the results obtained in the present work with the respective results[10,11] for the conventional fiber probe. It was shown that the use of a short Si core instead of a glass one allows us to achieve a strong enhancement in the transmission efficiency of up to 10^2-10^3.

(5) Although all calculations have been made in this work for the transverse-magnetic TM_{01} mode, our theoretical model assumes an extension on the case of the dominant transverse-electric TE_{11} mode. Since the eigenvalues $\nu_{11}(\theta_0)$ of this mode are somewhat lower than that for the TM_{01} mode, the resulting magnitudes of the transmission coefficient will be even higher than those obtained in this paper. In this case the advantages in the use of the Si core instead of a glass one will become some more evident.

ACKNOWLEDGMENTS

This work was supported in part by the Programme "Optical Spectroscopy and Frequency Standards" of the Division of Physical Sciences of the Russian Academy of Sciences and by the Russian Foundation for Basic Research (Project No. 02-02-16274). V. S. Lebedev acknowledges support from the Theory Institute for Strongly Correlated and Complex Systems at Brookhaven National Laboratory and is grateful for its hospitality.

*Electronic address: tkuzn@sci.lebedev.ru

[1] *Near-field Nano/Atom Optics and Technology*, edited by M. Ohtsu (Springer-Verlag, Berlin, 1998).
[2] B. Hecht, B. Sick, U. P. Wild, V. Deckert, R. Zenobi, O. J. F. Martin, and D. W. Pohl, J. Chem. Phys. **112**, 7761 (2000).
[3] C. Girard, C. Joachim, and S. Gauthier, Rep. Prog. Phys. **63**, 893 (2000).
[4] M. N. Islam, X. K. Zhao, A. A. Said, S. S. Mickel, and C. F. Vail, Appl. Phys. Lett. **71**, 2886 (1997).
[5] J. A. Veerman, A. M. Otter, L. Kuipers, and N. F. van Hulst, Appl. Phys. Lett. **72**, 3115 (1998).
[6] R. Eckert, J. M. Freyland, H. Gersen, H. Heinzelmann, G. Schürmann, W. Noell, U. Staufer, and N. F. de Rooij, Appl. Phys. Lett. **77**, 3695 (2000); J. Microsc. **202**, 7 (2001);
[7] A. Naber, D. Molenda, U. C. Fischer, H.-J. Maas, C. Höppener, N. Lu, and H. Fuchs, Phys. Rev. Lett. **89**, 210801 (2002).
[8] L. Novotny, D. W. Pohl, and B. Hecht, Opt. Lett. **20**, 970 (1995); Ultramicroscopy **61**, 1 (1995).
[9] H. Nakamura, T. Sato, H. Kambe, K. Sawada, and T. Saiki, J. Microsc. **202**, 50 (2001).
[10] T. I. Kuznetsova and V. S. Lebedev, Kvantovaya Elektron. (Moscow) **33**, 931 (2003) [Quantum Electron. **33**, 931 (2003)]; J. Russ. Laser Res. **24**, 458 (2003).
[11] T. I. Kuznetsova, V. S. Lebedev, and A. M. Tsvelik, J. Opt. A, Pure Appl. Opt. **6**, 338 (2004).
[12] P. Hoffman, D. Dutoit, and R.-P. Salanthé, Ultramicroscopy **61**, 165 (1995).
[13] D. Zeisel, S. Nettesheim, B. Dutoit, and R. Zenobi, Appl. Phys. Lett. **68**, 2491 (1996).
[14] R. Stöckle, C. Fokas, V. Deckert, R. Zenobi, B. Sick, B. Hecht, and U.P. Wild, Appl. Phys. Lett. **75**, 160 (1999).
[15] T. Yatsui, M. Kourogi, and M. Ohtsu, Appl. Phys. Lett. **71**, 1756 (1997).
[16] T. Yatsui, M. Kourogi, and M. Ohtsu, Appl. Phys. Lett. **73**, 2090 (1998).
[17] T. Saiki and K. Matsuda, Appl. Phys. Lett. **74**, 2773 (1999).
[18] L. Novotny and C. Hafner, Phys. Rev. E **50**, 4094 (1994).
[19] A. Castiaux, A. Dereux, J.-P. Vigneron, C. Girard, and O. J. F. Martin, Ultramicroscopy **60**, 1 (1995).
[20] A. Castiaux, C. Girard, A. Dereux, O. J. F. Martin, and J.-P. Vigneron, Phys. Rev. E **54**, 5752 (1996).
[21] E. Devaux, A. Dereux, E. Bourillot, J.-C. Weeber, Y. Lacroute, J.-P. Goudonnet, and C. Girard, Phys. Rev. B **62**, 10504 (2000).
[22] U. Schröter and A. Dereux, Phys. Rev. B **64**, 125420 (2001).
[23] H. U. Danzebrink, A. Castiaux, C. Girard, X. Bouju, and G. Wilkening, Ultramicroscopy **71**, 371 (1998).
[24] T. Dziomba, H. U. Danzebrink, C. Lehrer, L. Frey, T. Sulzbach, and O. Ohlsson, J. Microsc. **202**, 22 (2001).
[25] A. Castiaux, H. U. Danzebrink, and X. Bouju, J. Appl. Phys. **84**, 52 (1998).
[26] T. Yatsui, K. Isumi, M. Kourogi, and M. Ohtsu, Appl. Phys. Lett. **80**, 2257 (2002).
[27] T. I. Kuznetsova and V. S. Lebedev, Pis'ma Zh. Eksp. Teor. Fiz. **79**, 70 (2004) [JETP Lett. **79**, 62 (2004)].
[28] R. F. Harrington, *Time-Harmonic Electromagnetic Fields* (McGraw-Hill, New York, 1961).

[29] *Handbook of Mathematical Functions*, edited by by M. Abramowitz I. A. Stegun (Dover, New York, 1965).
[30] L. D. Landau, E. M. Lifshitz, and L. P. Pitaevskii, *Electrodynamics of Continuous Media*, 2nd ed. (Pergamon, Oxford, 1993).
[31] H. A. Bethe, Phys. Rev. **66**, 163 (1944).
[32] C. J. Bouwkamp, Rep. Prog. Phys. **17**, 35 (1954).
[33] T. I. Kuznetsova and V. S. Lebedev, Kvantovaya Elektron. (Moscow) **32**, 727 (2002) [Quantum Electron. **32**, 727 (2002)].
[34] A. Drezet, J. C. Woehl, and S. Huant, Phys. Rev. E **65**, 046611 (2002).
[35] D. E. Aspnes and A. A. Studna, Phys. Rev. B **27**, 985 (1983).